JOURNAL OF SOLID STATE CHEMISTRY 118, 227–240 (1995)

The Ferrites $Bi_{n+1}Sr_{2n+2}Ba_{n-1}Fe_{n+1}O_{6n+4}$: A Series of Intergrowths of the 2201 and 0201 Structures

M. Hervieu,* D. Pelloquin,* C. Michel,* M. T. Caldés,† and B. Raveau*

*Laboratoire CRISMAT-ISMRA et Université de Caen, Bd. du Maréchal Juin, 14050 Caen, Cedex, France; and †Instituto de Ciencia de Materiales de Barcelona (C.S.I.C.), Campus UAB, 08193-Bellaterra, Barcelona, Spain

Received November 11, 1994; in revised form February 21, 1995; accepted February 27, 1995

A new series of layered ferrites with the ideal formula $Bi_{n+1}Sr_{2n+2}Ba_{n-1}Fe_{n+1}O_{6n+4}$ has been synthesized. The ED and HREM studies of these phases show that they represent the three first members of a series of intergrowths of the 2201 ($Bi_2Sr_2CuO_6$-type) and 0201 (K_2NiF_4-type) structures. The parameters of their tetragonal cells are related to the a_p parameter of the perovskite and to the c_{2201} and c_{0201} parameters in the following way: $a \approx a_p$ and $c \approx \frac{1}{2}(c_{0201} + n.c_{2201})$ for the odd-n members or $c \approx c_{0201} + n.c_{2201}$ for the even-n members. The key point of this study deals with the stabilization of these structures by introducing barium on the bismuth sites. Problems of nonstoichiometry on the cationic sites in the bismuth layers and of oxygen nonstoichiometry are discussed. The disappearance of the modulation of the structure by introducing barium, as is in the 2212 cuprate $Bi_{1.5}Ba_{2.5}LaCu_2O_{8.25}$, is also evidenced and interpreted in terms of space for the $6s^2$ lone pair of Bi(III).

INTRODUCTION

Over the last several years, studies of the superconducting cuprates have allowed an extraordinary number of layered compounds derived from perovskite and rock salt structures to be generated (for a review see Ref. (1)). The high flexibility of copper coordination–octahedral, square pyramidal, square planar, tetrahedral—is at the origin of this phenomenon. Taking into consideration the latter property it should be possible to synthesize related oxides by replacing copper by another transition metal. In this respect, iron is a potential element since it exhibits several possible coordinations—octahedral, square pyramidal, tetrahedral—and several oxidation states—Fe(II), Fe(III), and Fe(IV). The recent discovery of three bismuth-based ferrites supports this viewpoint. The oxide $BiPbSr_2FeO_6$ (2) is indeed isotypic of $Bi_2Sr_2CuO_6$ (3–4), i.e., it can be described as a 2201 structure built up from triple-distorted rock salt layers $[(BiO)_2SrO]_\infty$ intergrown with single perovskite octahedral layers. In a similar way the ferrites $Bi_2Sr_3Fe_2O_9$ (5) and $Bi_2Sr_4Fe_3O_{12}$ (6) derive from the 2212 structure of $Bi_2Sr_2CaCu_2O_{8+\delta}$ (7–9) and the 2223 structure of $Bi_{2-x}Pb_xSr_2Ca_2Cu_3O_{10+\delta}$ (10–11), respectively. Nevertheless they differ from the corresponding cuprates by the absence of anionic vacancies in the perovskite layers, i.e., the layers of CuO_5 pyramids or CuO_4 square planar groups are replaced by layers of FeO_6 octahedra.

The investigation of the structural mechanism that governs the formation of these bismuth ferrites is very important since, like the superconducting bismuth cuprates, they exhibit an incommensurate modulated structure, with a periodicity along a which is close to $4.7 \times a_p\sqrt{2}$, whose origin is closely related to the stereoactivity of the $6s^2$ lone pair of Bi(III). Moreover, they are interesting for their magnetic properties owing to their bidimensional character. In order to understand nonstoichiometry in these bismuth ferrites, the system Bi–Sr–Ba–Fe–O has been explored further, bearing in mind the possibility of intergrowing the 2201 $Bi_2Sr_2CuO_6$-type structure (3–4) with the 0201 $SrLaFeO_4$-type structure (12). The introduction of barium in this system is based on the fact that this element substitutes easily for bismuth in the (BiO) layers, allowing a larger flexibility of this structure, as shown for the synthesis of the 2212 bismuth cuprate $Bi_{1.5}Ba_{2.5}LaCu_2O_{8.25}$ (13), which differs from the other 2212 bismuth cuprates by the absence of modulation. We report herein on new ferrites $Bi_{n+1}Sr_{2n+2}Ba_{n-1}Fe_{n+1}O_{6n+4}$, which represent the three first members of a series of intergrowths between the 2201 and 0201 structures. The possible substitution of calcium for strontium has also been investigated.

EXPERIMENTAL

Taking into account the general formula, $(Bi_2Sr_2FeO_6)_n(Sr_2FeO_4)$, several samples have been prepared, varying n from 1 to 3. For each sample, two types of substitution have been performed:

—Ca or Ba for strontium substitution according to the formulation $Bi_2Sr_{4-x}A_xFe_2O_{10}$ for $n = 1$ and $Bi_4Sr_{6-x}A_xFe_3O_{16}$ for $n = 2$, with A = Ca or Ba.

—barium for bismuth substitution according to the for-

0022-4596/95 $12.00

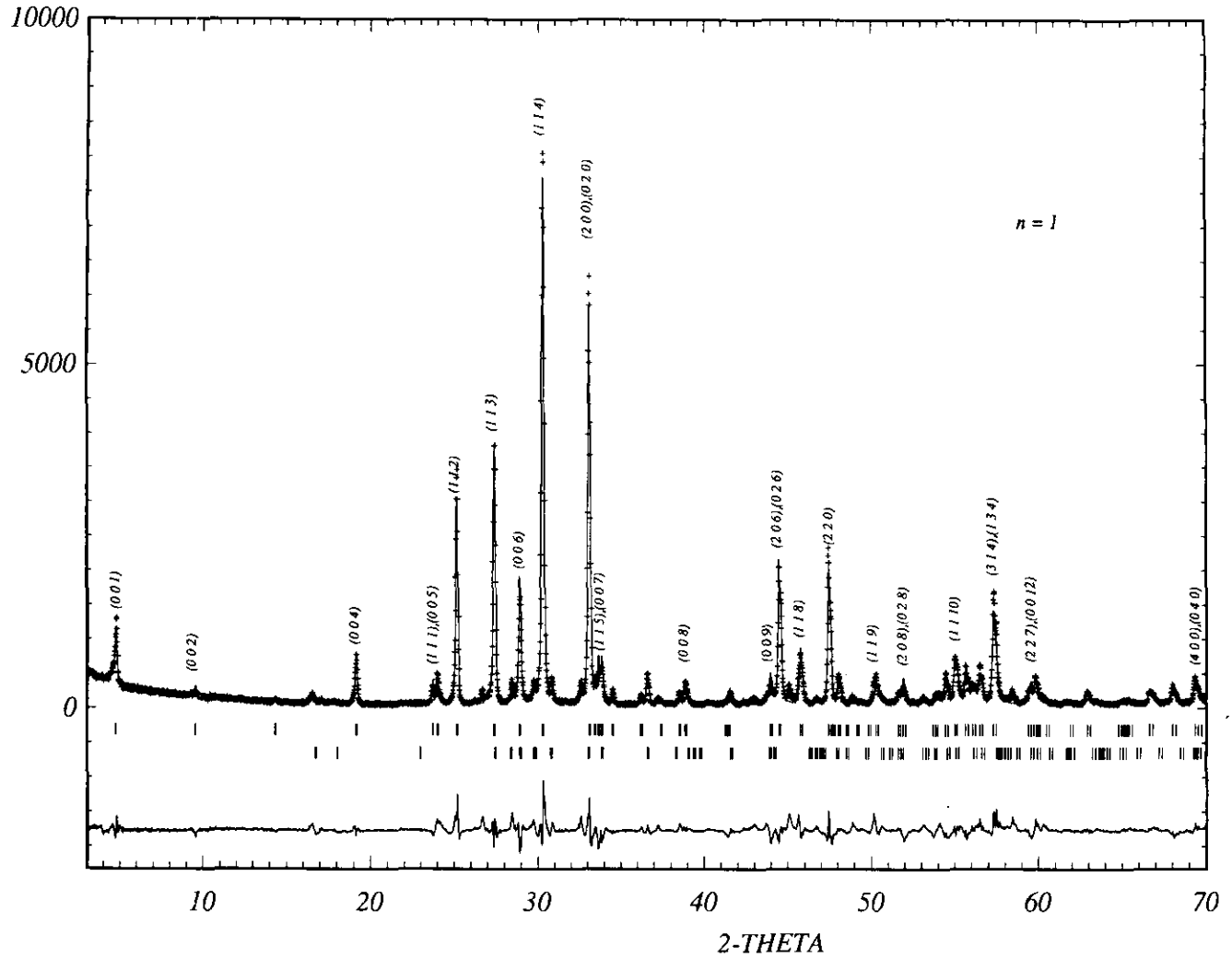

FIG. 1. X-ray diffraction pattern of $Bi_2Sr_4Fe_2O_{10}$ (strontium hydroxide has been added as a secondary phase).

mulation $Bi_{2-x}Ba_xSr_4Fe_2O_{10}$ for $n = 1$ and $Bi_{4-x}Ba_xSr_{6-x}Fe_3O_{16}$ for $n = 2$.

The samples have been prepared from stoichiometric mixtures of $BiONO_3$, $Sr(NO_3)_2$, and $BaCO_3$ or $Ca(NO_3)_2$, $4H_2O$, and Fe_2O_3 pressed in the form of bars and heated at temperatures ranging between 900 and 980°C, for 1 to 5 days. The thermal processes have been tested under air or N_2; the best results are obtained in air flow.

The X-ray diffraction (XRD) patterns have been registered on a Philips powder diffractometer using Cu$K\alpha$ radiation. Data were collected by step-scanning with increments of 0.02° (2θ). Lattice parameters and structures were refined using a Rietveld method (computer program FULLPROF (14)).

The electron diffraction (ED) investigation was carried out on a JEOL 200CX electron microscope, and the high resolution electron microscopy (HREM) study was carried out on a TOPCON 002B, operating at 200 KV and having a point resolution of 1.8 Å. Images were recorded with an objective lens aperture radius of 0.7 $Å^{-1}$; image calculations were carried out using the multislice method of the EMS program. The samples were prepared by crushing the crystals in alcohol and the grains were deposited on a holey carbon film. EDX analyses were systematically performed, taking $Bi_2Sr_2CuO_6$, $SrFeO_{3-x}$, $BaBiO_3$, and Ca_2CuO_3 as standards.

RESULTS AND DISCUSSION

The First Member of the Series: $Bi_2Sr_{4-x}Ca_xFe_2O_{10}$

The powder X-ray diffraction pattern of the limit phase $Bi_2Sr_4Fe_2O_{10}$ (Fig. 1) confirms the powder data previously given by Mayer *et al.* (15). The reconstruction of the reciprocal space from the ED patterns (Fig. 2) evidences an orthorhombic symmetry in spite of the very close values of the *a* and *b* parameters. Thus this oxide is character-

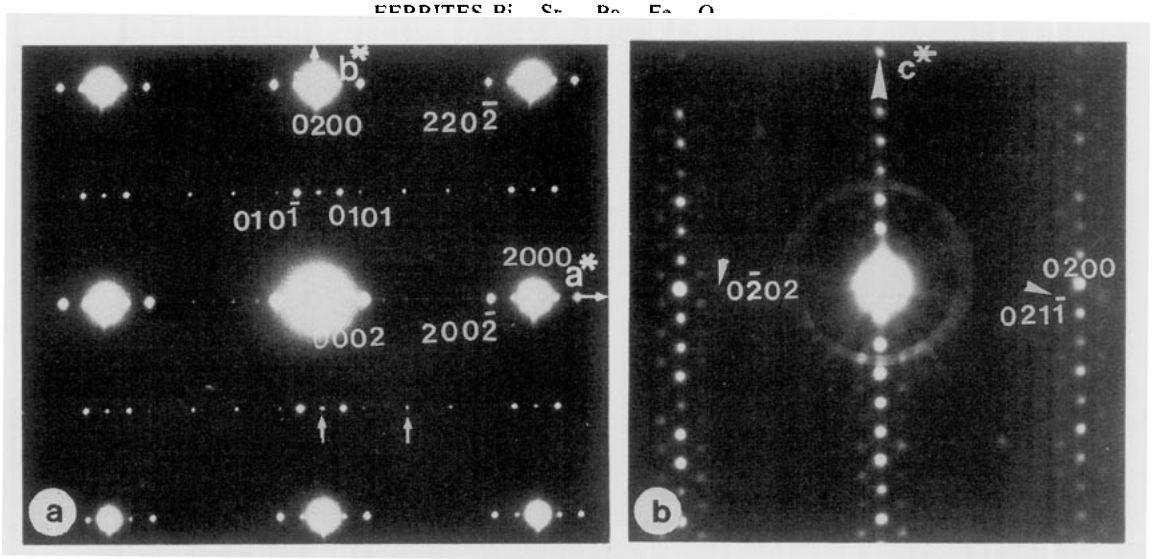

FIG. 2. ED patterns of $Bi_2Sr_4Fe_2O_{10}$ where the different spots are indexed using four indices. (a) [001]: the small white arrows show two examples of weak intensities which are attributed to the upper levels of the reciprocal space; they correspond to the reflections $0\bar{1}10$ and $1\bar{1}1\bar{1}$. (b) [010]: the white arrowheads indicate the satellites which are indexed.

TABLE 1
$Bi_2Sr_{4-x}Ca_xFe_2O_{10}$: Subcell Parameters

x	a (Å)	b (Å)	c (Å)
0	5.420(2)	5.412(2)	18.549(1)
0.15	5.414(2)	5.414(2)	18.524(1)
0.6	5.405(4)	5.406(4)	18.418(2)
0.7	5.405(5)	5.403(5)	18.382(4)

ized by the orthorhombic subcell $a \approx b \approx a_p\sqrt{2}$, and $c \approx 18.5$ Å, with hkl, $h + k = 2n$ and $hk0$, $h, k = 2n$ as conditions limiting the reflection and involving $Cm2a$ and $Cmma$ as possible space groups (a_p being the parameter of the cubic perovskite cell). The substitution of calcium for strontium allows a solid solution $Bi_2Sr_{4-x}Ca_xFe_2O_{10}$, with a large homogeneity range $0 \leq x \leq 0.7$, to be isolated. The values of the cell parameters (Table 1) show that the a and b parameters do not differ from each other, regardless of the value of x, but that c decreases signifi-

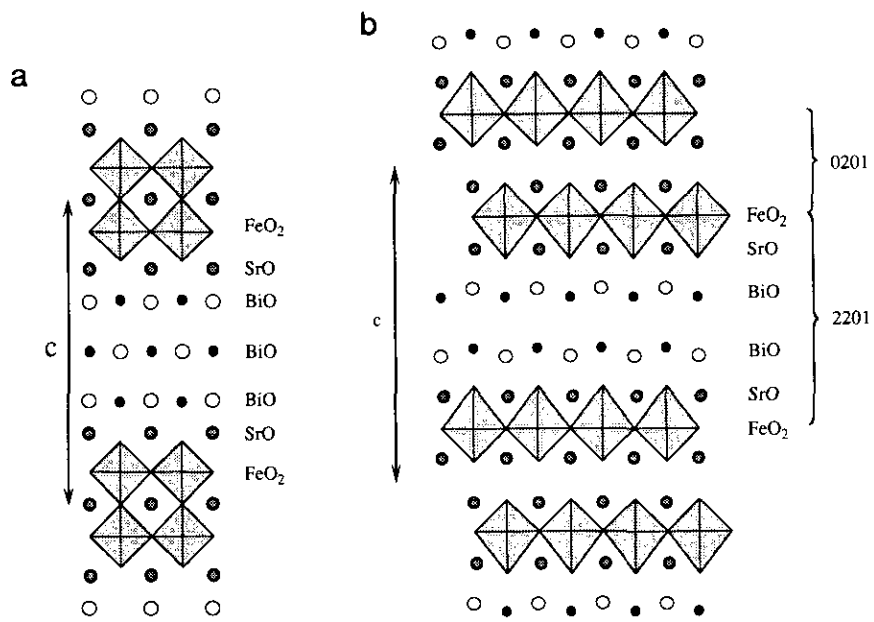

FIG. 3. Idealized drawing of $Bi_2Sr_4Fe_2O_{10}$. (a) model proposed by Mayer *et al.* (b) model proposed in this paper corresponding to the intergrowth of 2201 and 0201 units.

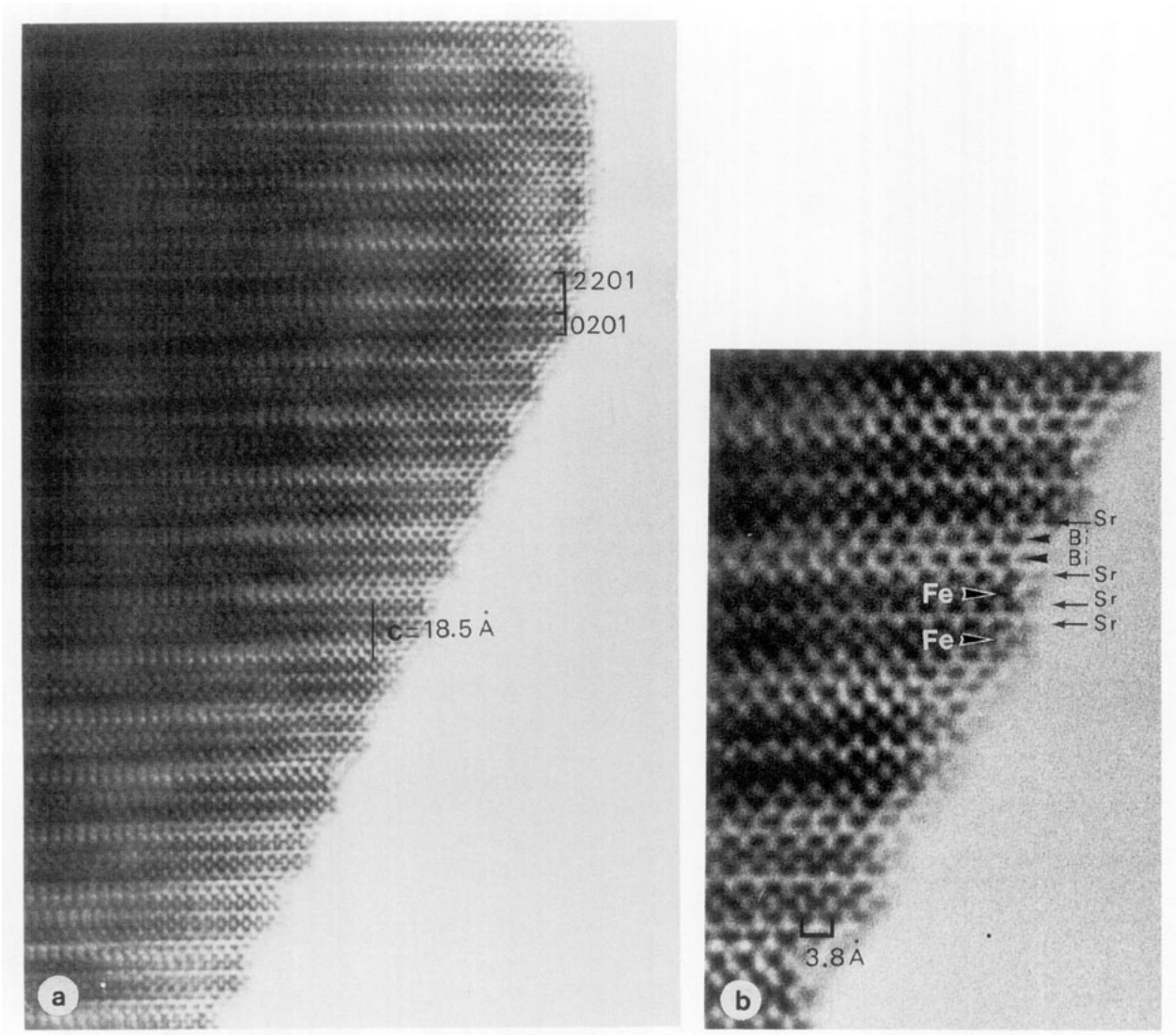

FIG. 4. [110] HREM images of $Bi_2Sr_4Fe_2O_{10}$. (a) overall image showing the regularity of the layer stacking. (b) enlarged image where cation positions appear as dark spots.

TABLE 2
$Bi_{1.8}Sr_{3.85}Ca_{0.15}Fe_2O_{10}$: Structural Data ($Z = 2$; S.G. = $Cm2a$; $R_i = 0.096$)

	Site	x	y	z	B (Å^2)	N
Bi	4c	0.25	0.0	0.4185(2)	1.8(1)	3.54(2)
Sr (1)	4c	0.25	0.535(3)	0.2652(3)	1.8(4)	3.60(6)
Ca (1)	4c	0.25	0.535(3)	0.2652(3)	1.8(4)	0.40(6)
Sr (2)	4c	0.25	0.5	0.0697(4)	0.9(2)	4
Fe	4c	0.25	0.0	0.1606(5)	0.1(2)	4
O (1)	4c	0.25	0.0	0.060(1)	1	4
O (2)	8d	0.0	0.25	0.1615(11)	1	8
O (3)	4c	0.25	0.0	0.297(1)	1	4
O (4)	8d	0.381(6)	0.631(6)	0.392(2)	1	4

TABLE 3
$Bi_{1.8}Sr_{3.85}Ca_{0.15}Fe_{12}O_{10}$: Interatomic Distances

Bi–0(3)	2.24(3) × 1	Sr(2)–0(1)	2.71(1) × 4
Bi–0(4)	2.17(3) × 2	Sr(2)–0(1)	2.41(3) × 1
		Sr(2)–0(2)	2.56(2) × 4
(Sr,Ca)1–0(2)	2.81(2) × 2		
(Sr,Ca)1–0(2)	2.62(2) × 2		
(Sr,Ca)1–0(3)	2.59(2) × 1	Fe–0(1)	1.86(3) × 1
(Sr,Ca)1–0(3)	2.78(1) × 2	Fe–0(2)	1.91(0) × 4
(Sr,Ca)1–0(3)	2.96(2) × 1	Fe–0(3)	2.54(3) × 1
(Sr,Ca)1–0(4)	2.51(4) × 1		

cantly as x increases, in agreement with the smaller size of calcium compared to strontium.

At this stage of the investigation, two models can be considered for this structure. The first one (Fig. 3a) corresponds to an intergrowth of double octahedral perovskite layers $[SrFeO_3]_\infty$ with quadruple-distorted rock salt layers $[(BiO)_2(SrO)_2]_\infty$ proposed by Mayer *et al.* (15). The second model (Fig. 3b) consists of an intergrowth of single 2201-type layers, i.e., $Bi_2Sr_2CuO_6$-type layers and 0201-type layers, i.e., K_2NiF_4-type layers. Although the two structures are fundamentally different, the stacking of the cationic sequences along $\vec{c}$, Fe–Sr–($^{Bi}_{Sr}$)–Bi–($^{Bi}_{Sr}$)–Sr–Fe–Sr–Fe for the first one and Fe–Sr–Bi–Bi–Sr–Fe–Sr–Sr–Fe for the second one suggests that it should be difficult to decide between these two models from only powder X-ray data, especially if one takes into consideration the presence of satellites in incommensurate positions visible on the [001] (Fig. 2a) and [010] (Fig. 2b) ED patterns, with a modulation vector along a^* of 1/4.9. For the layered bismuth copper and iron oxides, a four-dimensional notation is commonly used when indexing reciprocal space points (16); the modulated structure exhibits an orthorhombic cell with $a_{mod} \approx q.a_p\sqrt{2}$, $b_{mod} \approx a_p\sqrt{2}$,

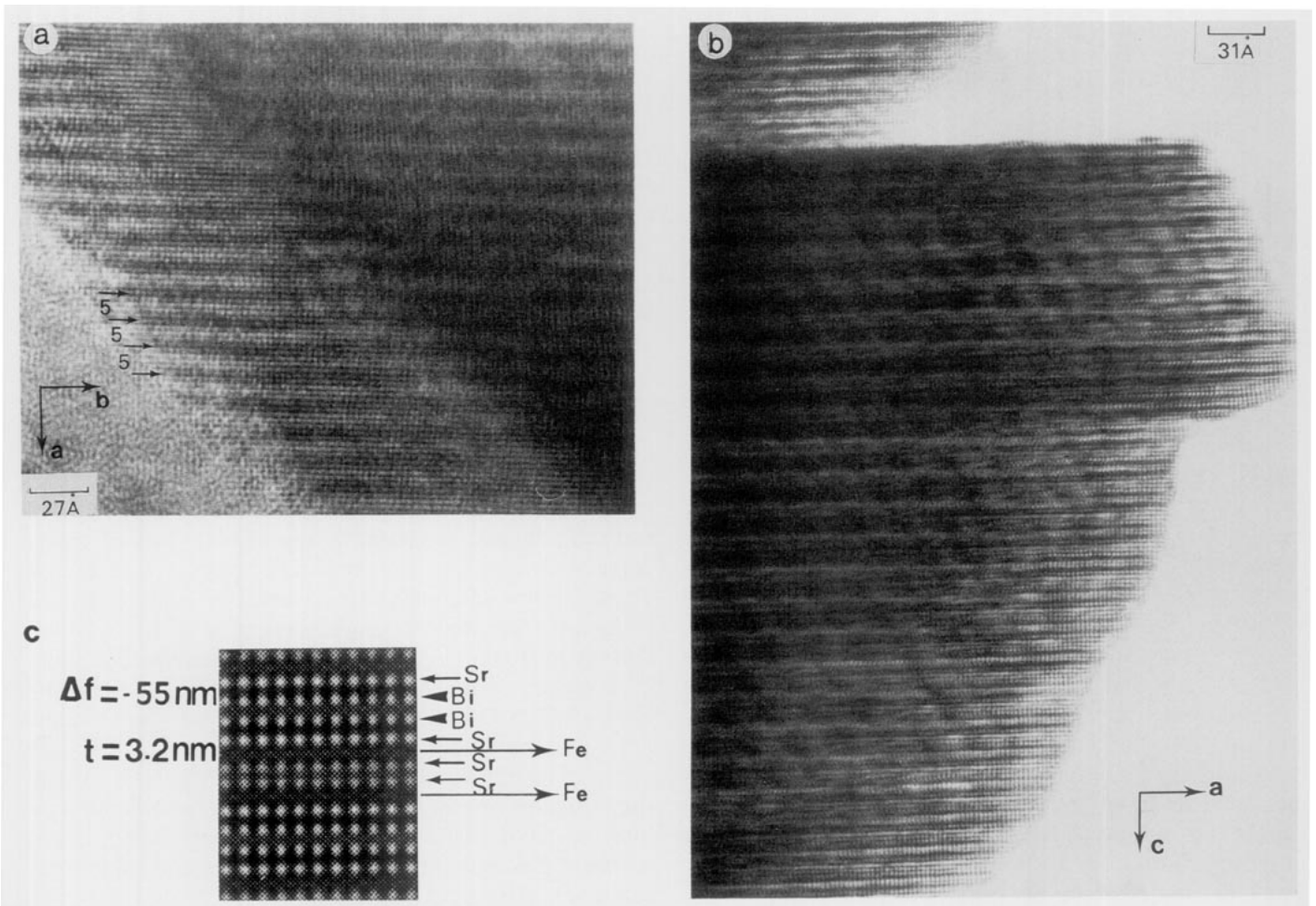

FIG. 5. (a) [010] HREM image attesting the regularity of the periodicity along $\vec{a}$ and showing the undulation of the layers. The [BiO] and the [SrO] layers are imaged as rows of bright spots. (b) theoretical image calculated for a nonmodulated subcell: $\Delta f = -55$ nm and crystal thickness 3.2 nm. (c) [010] projection of the idealized structure.

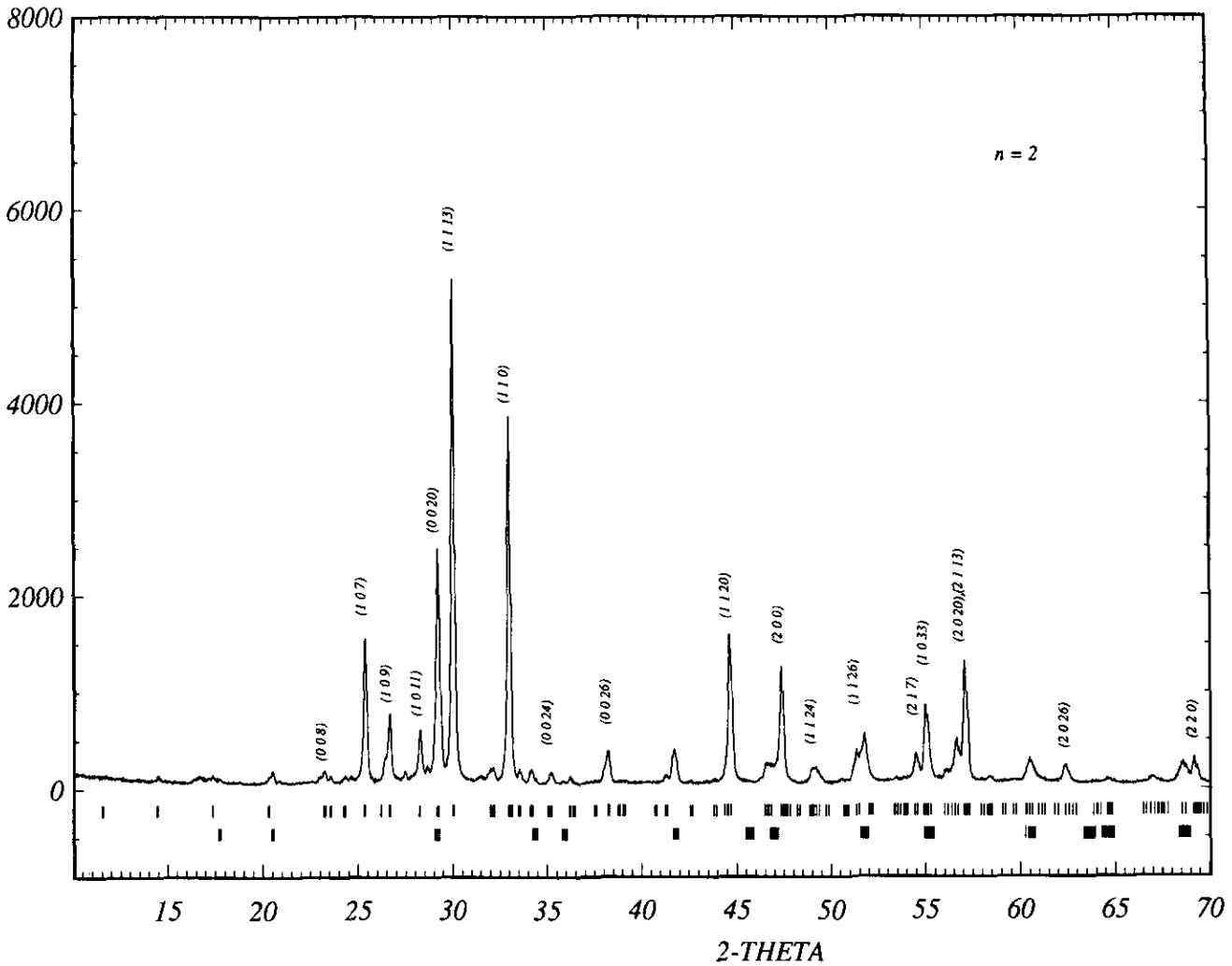

FIG. 6. X-ray diffraction pattern of $Bi_3BaSr_6Fe_3O_{16}$ ($BaBiO_3$ has been added as a secondary phase).

and $c_{mod} = 2 \times 18.5$ Å and conditions limiting the reflection, $hklm$, $h + k + l + m = 2n$. It should be noted that the weak intensity of the forbidden reflections, which are often observed in the [001] patterns of the lamellar bismuth cuprates, is attributed to upper levels of the reciprocal lattice (17); two examples are indicated by small white arrows in Fig. 2a.

Conversely, a HREM investigation should allow the two different stackings of the layers to be easily distinguished. Thus the identification of the layers along $\vec{c}$ is deduced from [110] images, whereas [010] and [001] images give information about the modulation. Note that the crystals exhibit a highly lamellar morphology already observed for the bismuth cuprates and also for $Bi_2Sr_3Fe_2O_9$ (5) and $Bi_2Sr_4Fe_3O_{12}$ (6).

An overall [110] image is given in Fig. 4a, which attests to the high regularity of the layer stacking, and an enlarged image is given in Fig. 4b, where the cation positions appear as dark spots. The two rows of darkest spots are correlated to the double bismuth layers; they are surrounded, on each side, by rows of dark spots correlated to $[SrO]_\infty$ layers. A second group of two rows of spots, correlated in the same way to $[SrO]_\infty$ layers, are observed. These groups of four and two rows of staggered dark spots are separated by single rows of grey spots which correspond to the $[FeO_2]_\infty$ layers. Thus the sequence along $\vec{c}$ is clearly evidenced as FeO_2–SrO–BiO–BiO–SrO–FeO_2–SrO–SrO–FeO_2, corresponding to the second structural model described in Fig. 3b.

These results discard the first model (Fig. 3a), so that the structure of this phase (Fig. 3b) can be described as built up from single $[SrFeO_3]_\infty$ perovskite layers intergrown with single $[SrO]_\infty$ rock salt layers and triple rock salt layers $[(BiO)_2SrO]_\infty$, alternately. Note that the existence of five consecutive $[AO]_\infty$ layers, as in the first model, has never been observed in the course of HREM investigation, even in the form of extended defects.

The EDX analysis performed on numerous crystals

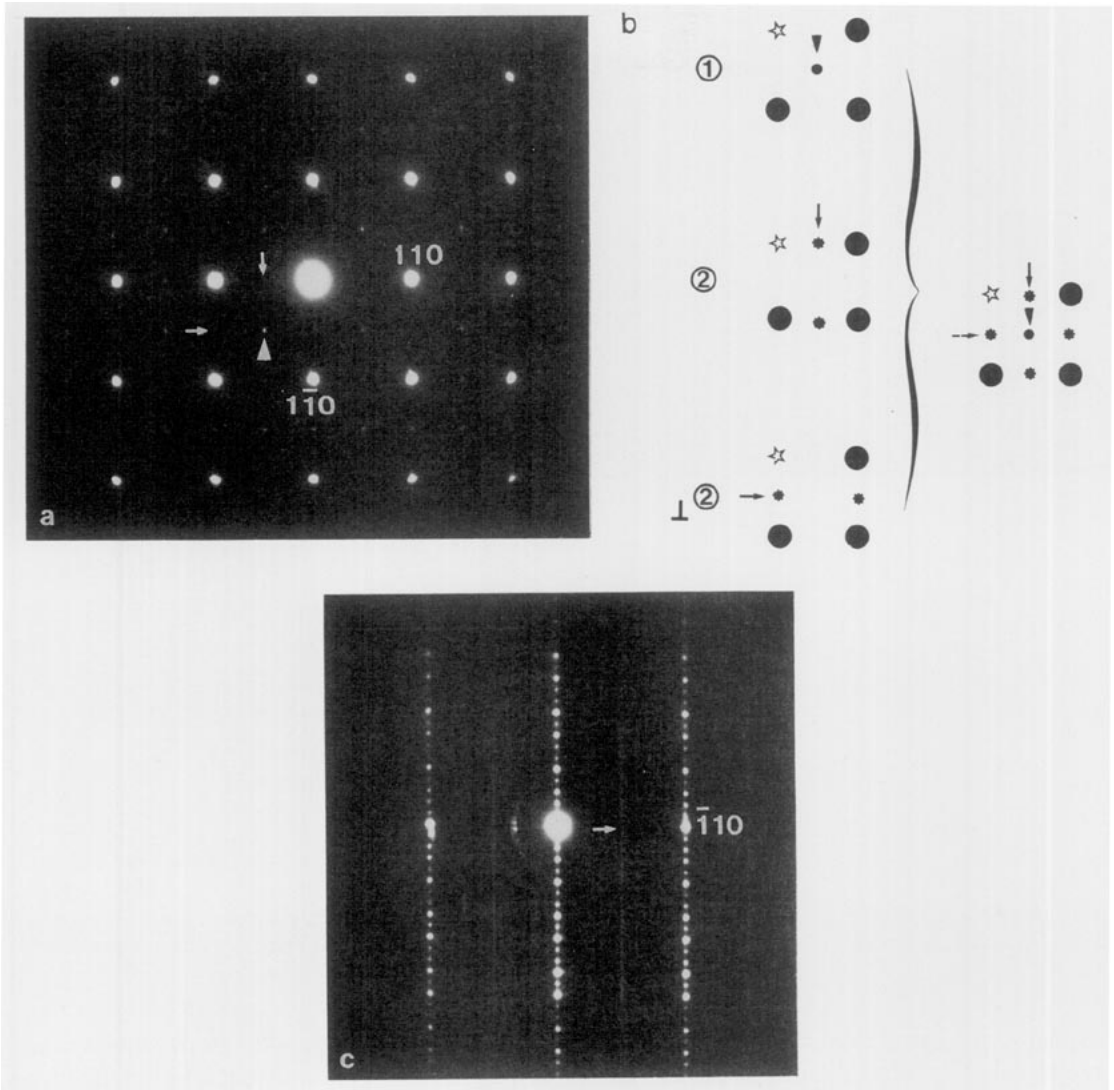

FIG. 7. ED patterns of $Bi_3BaSr_6Fe_3O_{16}$. (a) [001] pattern. The additional reflections corresponding to a *P*-type tetragonal cell are shown by a white arrowhead. The small arrows indicate the existence of weak reflections corresponding to an orthorhombic cell. (b) Schematic drawing of the [001] ED pattern showing the superposition of the different systems. (c) [110] ED pattern. Weak diffuse extra reflections (white arrow) are observed which violate the I-type symmetry.

shows that a small bismuth deficiency is systematically observed, so that the actual formula should be written $Bi_{2-\delta}Sr_{4-x}Ca_xFe_2O_{10}$, with $\delta \approx 0.2$.

Although they are not highly significant, structure calculations from powder X-ray data are interesting for the determination of the positions of heavy atoms that can be used in a second step for HREM image simulations. Using all possible reflections contained in the angular range $3° \leq 2\theta \leq 70°$, i.e., 79 *hkl*, the positional parameters of the phase $Bi_2Sr_{3.85}Ca_{0.15}Fe_2O_{10}$ were first refined. Then the occupancy factors and thermal factors of the cations were refined, the thermal factors of the oxygen atoms being fixed to 1 $Å^2$, and these anionic sites being considered as fully occupied. The R_i factor was lowered to 0.096, which can be considered as reasonable for an average structure, if one takes into account its incommensurate modulation. The corresponding crystallographic data (Table 2) show that the refinement of the occupancy factors are in agreement with the EDX analysis, as well about the bismuth deficiency as about the calcium content, the latter being located in the strontium layers adjacent to the bismuth layers. The interatomic distances (Table 3) are close to those usually observed for this kind of oxide. Note the particular geometry of FeO_6 octahedra that exhibit an abnormally short apical bond (1.86 Å), the opposite bond being abnormally long (2.54 Å), so that the coordination of Fe(III) can also be described as square pyramidal, or 4 + 1. Such behavior is not particular to this ferrite and

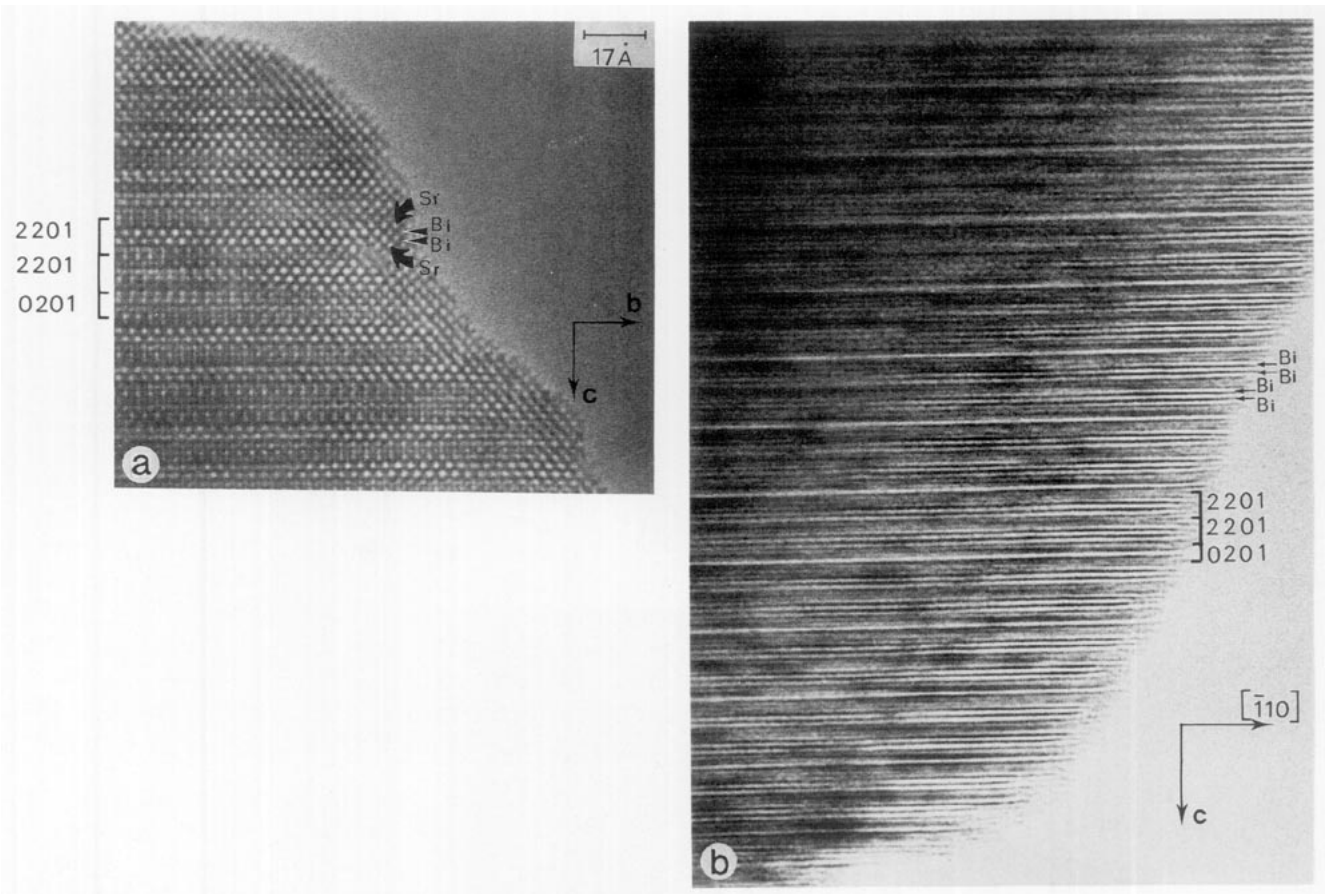

FIG. 8. (a) [100] HREM image of $Bi_3BaSr_6Fe_3O_{16}$ showing the layer stacking. The heavy atom positions appear as white spots. The [BiO] layers are represented by black arrowheads. (b) [110] HREM image. The [BiO] layers are imaged as black rows. Note the existence of distortions of the layers.

has previously been observed from neutron diffraction studies in several other layered ferrites such as $PbSr_4Fe_2O_9$ (18).

The [010] HREM images (Fig. 5a) show that the modulation is very regularly established throughout the whole matrix. Such images are characterized by the existence of two groups of four and two rows of bright spots, separated by single dark rows. The bright spots are aligned along $\vec{c}$ when the structure is viewed along that direction (Fig. 5c). In order to identify the nature of the different layers viewed along that direction, simulated images, calculated from the refined positions of Table 2 for a nonmodulated subcell, have been performed (Fig. 5b); they show that the rows of bright spots are correlated to the Bi and Sr rows. In that micrograph, undulations of the different layers, with a periodicity of ≈26.6 Å along a and ≈37 Å along c, is perfectly observed, leading to a centered image in the thick part of the crystal. These undulations of the layers have been shown to be directly a related to the existence of modulations in the bismuth strontium compounds. The structural studies of the 2201 cuprates (19) showed indeed that both a displacive modulation wave, acting on all atoms, and a density modulation wave, governing the occupancy probabilities of the Bi, Sr, and apical O(2) sites, are involved in the crystals; the numerous HREM studies which have been performed on the 2201 and 2212 compounds show that the undulations of the layers which result from the displacive modulations, as well as their evolutions with the material composition, are clearly observed (17, 20, 21); similar features have been reported in the 2212 and 2223 iron-based phases (5, 6). It is interesting to note that the double [SrO] layers of the 0201 unit are also strongly waving.

Note that all attempts to partially replace bismuth or strontium by barium in this phase were unsuccessful. Thus $Bi_{2-\delta}Sr_{4-x}Ca_xFe_2O_{10}$ appears as the first member of a series of ideal intergrowth $(Bi_2A_2Fe_2O_6) \cdot A_2FeO_4$, with A = Sr, Ca.

The Second Member of the Series: $Bi_3BaSr_6Fe_3O_{16}$

In order to realize the second member of the ideal intergrowth series, compositions corresponding to the formula $Bi_4Sr_{6-x}A_xFe_3O_{16}$ were explored for A = Ca, Ba. Regard-

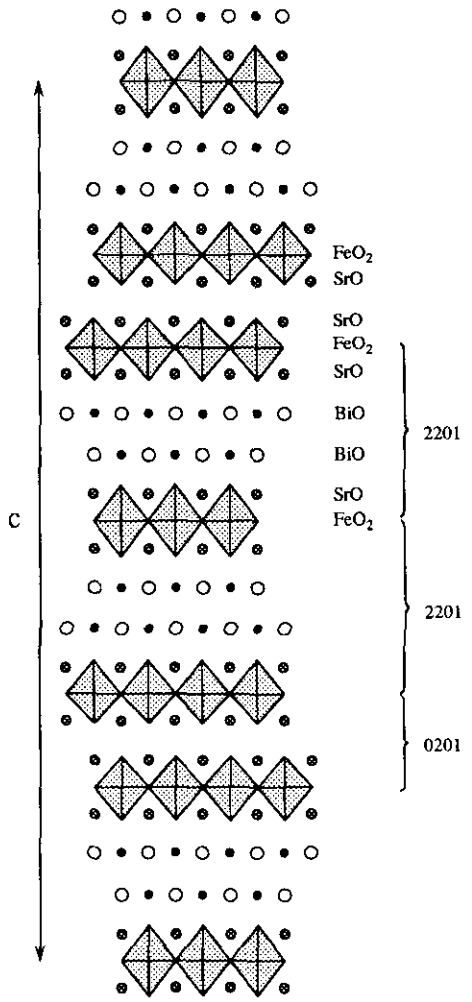

FIG. 9. Idealized model of the second member of the series $Bi_3BaSr_6Fe_3O_{16}$.

TABLE 5
$Bi_3BaSr_6Fe_3O_{16}$: Interatomic Distances

(Bi, Ba)1–0(2)	2.28(7) × 1	Sr(2)–0(4)	2.73(1) × 1
(Bi, Ba)1–0(3)	2.71(0) × 4	Sr(2)–0(5)	2.75(1) × 4
(Bi, Ba)1–0(4)	2.89(1) × 1	Sr(2)–0(6)	2.69(3) × 4
(Bi, Ba)2–0(3)	2.89(1) × 1	Sr(3)–0(6)	2.64(3) × 4
(Bi, Ba)2–0(4)	2.71(0) × 4	Sr(3)–0(7)	2.72(1) × 4
(Bi, Ba)2–0(5)	2.26(6) × 1	Sr(3)–0(7)	2.56(7) × 1
		Fe(1)–0(1)	1.92(0) × 4
		Fe(1)–0(2)	2.29(7) × 2
Sr(1)–0(1)	2.68(1) × 4	Fe(2)–0(5)	2.37(7) × 1
Sr(1)–0(2)	2.75(1) × 4	Fe(2)–0(6)	1.92(0) × 4
Sr(1)–0(3)	2.70(1) × 1	Fe(2)–0(7)	2.05(8) × 1

less of the value of A or x, no phase exhibiting the expected XRD pattern was identified. At this stage the possibility of stabilizing this member by introducing barium on the bismuth site was considered. A new phase, $Bi_3BaSr_6Fe_3O_{16}$, was isolated, whose powder XRD pattern (Fig. 6) is closely related to that of $Bi_2Sr_4Fe_2O_{10}$. The EDX analysis of this phase confirmed its composition. The reconstruction of the reciprocal space by ED evidences a tetragonal subcell with $a = b = a_p$, $c \approx 61$ Å, and an I-type space group. From the [001] and [110] ED patterns (Fig. 7), one remark must be made dealing with the existence of very weak extra reflections which attest that the I-type tetragonal symmetry is violated. The existence of similar weak reflections in the nonmodulated lead-doped 2212 cuprates have been reported (23, 24); several hypotheses, such as the oxygen content or cell distortions, have been proposed to explain their origin. In the case of $Bi_3BaSr_6Fe_3O_{16}$, they can be described from the superposition of two systems; the first one corresponds to a P-type

TABLE 4
$Bi_3BaSr_6Fe_3O_{16}$: Structural Data (S.G.: $I4/mmm$; $R_i = 0.111$)

	Site	x	y	z	B	N
(Bi/Ba)1	4*e*	0	0	0.5746(1)[a]	1.9(2)[d]	3/1
(Bi/Ba)2	4*e*	0	0	0.1219(1)[b]	1.9(2)[d]	3/1
Sr(1)	4*e*	0	0	0.0305(2)	−0.5(3)[e]	4
Sr(2)	4*e*	0	0	0.6666(2)	−0.5(3)[e]	4
Sr(3)	4*e*	0	0	0.7271(3)	−0.1(3)	4
Fe(1)	2*b*	0	0	1/2	2.5(9)	2
Fe(2)	4*e*	0	0	0.1875(3)[c]	2.6(9)	4
O(1)	4*d*	0	1/2	0	1.0	4
O(2)	4*e*	0	0	0.5404(12)	1.0	4
O(3)	4*e*	0	0	0.0746(1)[a]	1.0	4
O(4)	4*e*	0	0	0.6219(1)[b]	1.0	4
O(5)	4*e*	0	0	0.1588(10)	1.0	4
O(6)	4*g*	0	1/2	0.1875(3)[c]	1.0	8
O(7)	4*e*	0	0	0.2311(11)	1.0	4

[a,b,c] The z value of (Bi, Ba)1 and O(3), (Bi, Ba) and O(4), and Fe(2) and O(6) were constrained.
[d,e] The B value of (Bi, Ba)1 and (Bi, Ba)2 and Sr(1) and Sr(2) were constrained due to similar environment.

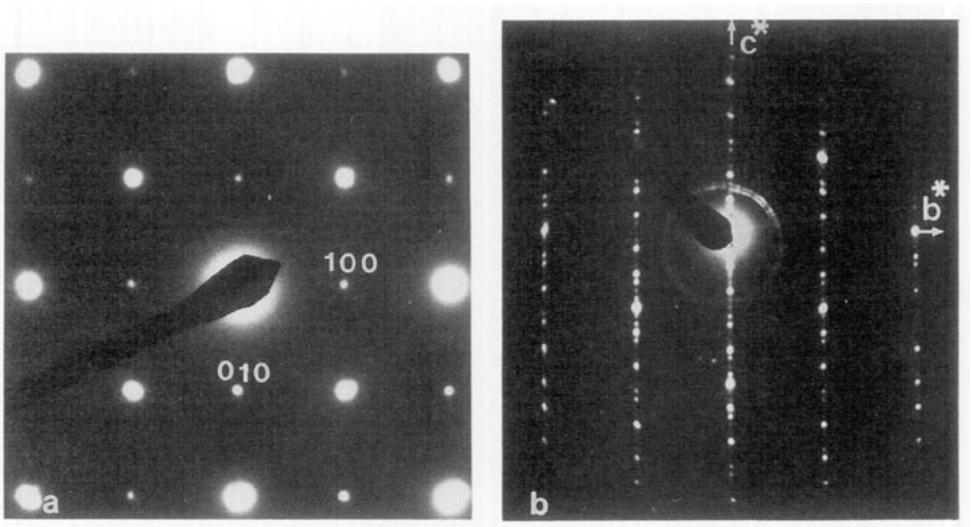

FIG. 10. (a) [001] and (b) [100] ED patterns of the third member, $Bi_4Ba_2Sr_8Fe_4O_{22}$.

tetragonal cell with $a \approx a_p$ (white arrowhead in Fig. 7a) and the second corresponds to an orthorhombic cell with $a \approx b \approx a_p\sqrt{2}$ and the limiting condition of reflection $hk0$, $h = 2n$ (small arrow in Fig. 7a). In the latter system, note that a twinning phenomenon is quite systematically observed, as shown in the schematical drawing in Fig. 7b.

Nevertheless the cell parameters were refined from the XRD pattern to $a = 3.837(1)$ Å and $c = 61.16(1)$ Å.

The [100] HREM images (Fig. 8a) allow the layer sequences to be checked. In that enlarged image where the cation positions appear as staggered rows of bright spots, one observes a sequence of two groups of four rows of bright spots [–SrO–(Bi,Ba)O–(Bi, Ba)O–SrO] which alternate with a group of two rows of bright spots (SrO–SrO), separated by single rows of grey spots (FeO_2). These observations allow a structural model to be proposed (Fig. 9).

Thus this structure can be described as an intergrowth of double 2201 layers $[(Bi_{1.5}Ba_{0.5}Sr_2FeO_6)_2]_\infty$ with single 0201 layers $[Sr_2FeO_4]_\infty$.

The large cell dimensions and the large number of variable parameters to be refined allow only an average structure to be calculated. Calculations were performed in the space group I_4/mmm and in the tetragonal cell a_pxa_pxc using the 95 reflections included in the angular range $3° \leq 2\theta \leq 70°$. To minimize the number of variables and taking in account structural considerations, some positional parameter and B factors were constrained (see Table 4). No splitting from the ideal position of the oxygens belonging to the (Bi, Ba) plane (O(3) and O(4)) was considered. Using the same sequence of refinements and similar conditions for B and occupancy factors of oxygen atoms, the structure of this phase could be refined to $R_i = 0.11$ for the positional parameters and interatomic distances given in Tables 4 and 5, respectively. These results are thus in agreement with the HREM observations. Note that the rather high R_i value and the slightly negative B values obtained for Sr atoms are not only due to the lack of information but are also the result of the presence of extended defects. The stacking of the layers along $\vec{c}$ is indeed not so regular as in the first member, as shown in Fig. 8a. Moreover in the [110] images (Fig. 8b), one observes that the structure is no longer modulated but that there numerous local distortions of the layers which may cause the streaks along $\vec{c}^*$.

The Third Member of the Series: $Bi_4Ba_{2-\delta}Sr_8Fe_4O_{22}$

In order to synthesize the third member of the series, the nominal compositions $[Bi_{1.5-x}Ba_{0.5+x}Sr_2FeO_6]_3$ Sr_2FeO_4 were explored, varying x from 0 to 0.5. The best results were obtained for $x \approx 0.2$. The ED investigation shows that the $n = 3$ member appears in a majority of crystals in the form of a very regular stacking. The EDX analysis shows that the cationic ratio is not far from the nominal composition, although it exhibits a rather significant barium deficiency, i.e., $Bi_4Ba_{1.5}Sr_8Fe_4$, with respect to the ideal composition $Bi_4Ba_2Sr_8FE_4O_{22}$ that satisfies the charge balance.

The presence of other members, as well as other related compounds, as impurities or as extended defects in the $n = 3$ matrix prevents the cell parameters from being refined, due to the overlap of peaks. Nevertheless the ED and HREM study of regular crystals of this new phase allows its structure to be identified.

The reconstruction of reciprocal space for crystals of the $n = 3$ type evidences a tetragonal subcell with $a_p \approx 3.85$ Å and $c \approx 42.6$ Å. A [100] ED pattern is shown in Fig. 10b, where the sharpness of the reflections attests the layer ordering, as confirmed with the corresponding

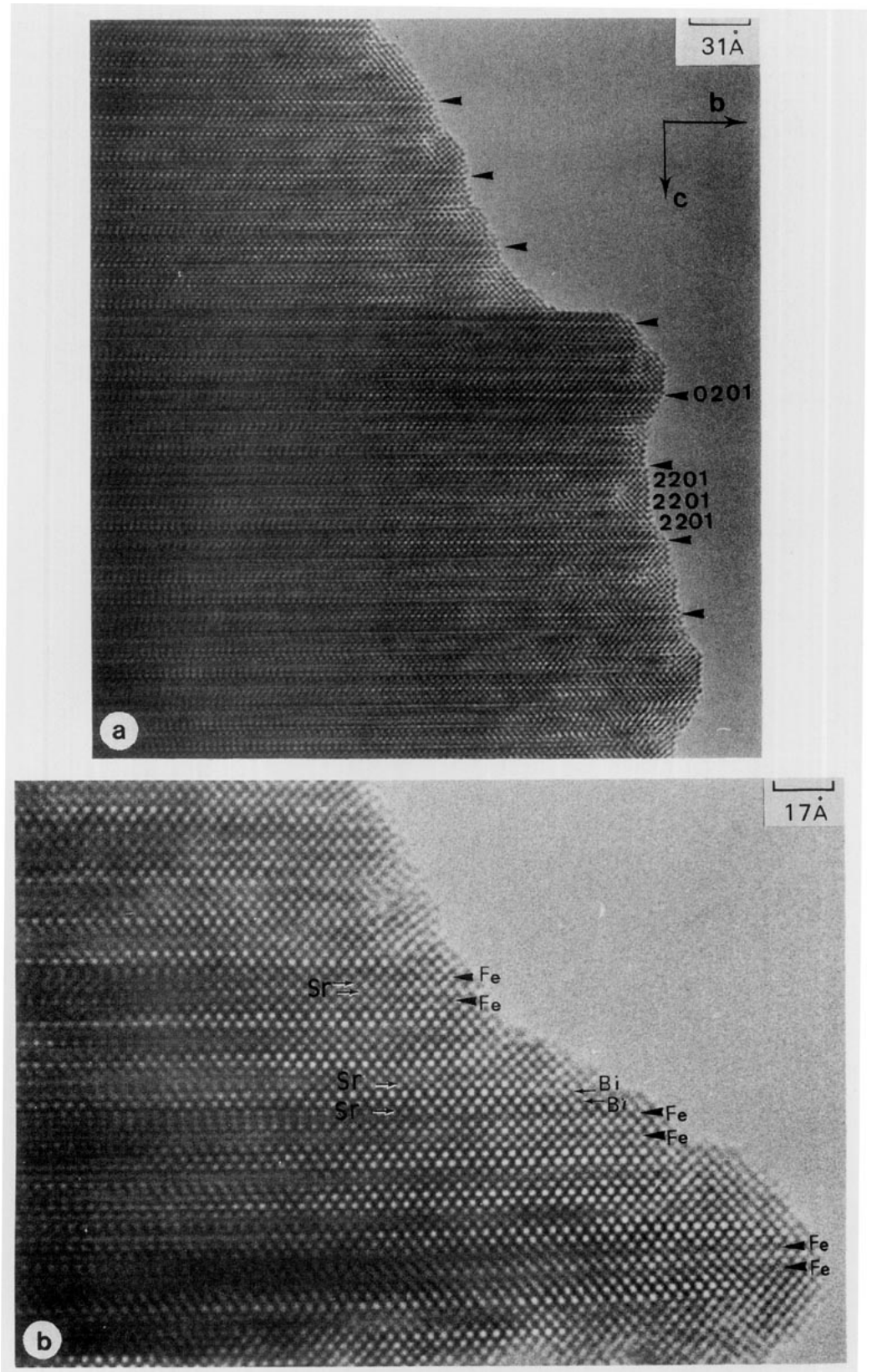

FIG. 11. (a) [100] HREM image of $Bi_4Ba_2Sr_8Fe_4O_{22}$ attesting to the layer ordering. Black arrows indicate the $[SrO]_2$ double layer of the 0201 units. (b) Enlarged image showing the layer stacking. The cation positions appear as bright spots.

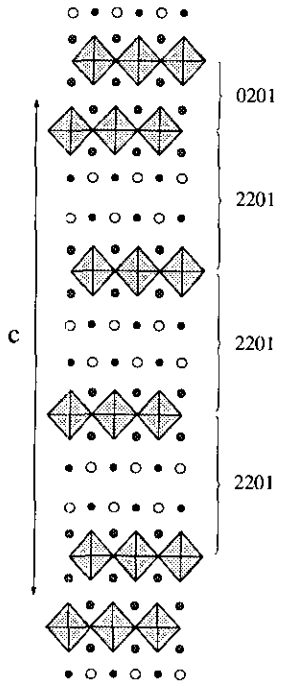

FIG. 12. Idealized model of the third member of the series $Bi_4Ba_2Sr_8Fe_4O_{22}$.

images (Fig. 11a). In the enlarged images (Fig. 11b) where the cation positions appear as bright spots, one observes a sequence of three groups of four rows of staggered bright spots, correlated to the Sr–(Bi,Ba)–(BiBa)–Sr sequence, and one double row of bright spots, Sr–Sr; they are separated by single rows of grey spots, the iron layers. Thus, the structure corresponds to the member $n = 3$ of the family; it is built up from the intergrowth of three 2201 units with one 0201 unit (Fig. 12). Note also that this member, as the $n = 2$ member, does not exhibit any modulation of the structure (Fig. 11a).

Extended Defects and Modulation

If the sequence of the layer stacking is highly regular in the member $n = 1$, the intergrowth defects begin to be observed as soon as $n > 1$; it results in aleatory sequences of $n = 1$, 2, 3, and 4 members (Fig. 13). Members with n greater than 4 have not been observed for that composition; in the same way, two adjacent 0201 units, which would correspond to the member $m = 2$, have not be detected.

A second feature is systematically observed (Fig. 13) when the $n = 2$, 3, and 4 members coexist. It deals with the fact that the $n = 2$ and 3 members are not modulated, whereas the $n = 4$ member exhibits a modulation. The EDX analysis performed at the level of this defect shows a significant local decrease of the barium content, with Ba/Bi inferior to 0.2; such a feature results indeed from a local inhomogeneity of the cation distribution but is consistent with the role of the barium for bismuth substitution which, similarly to the lead for bismuth substitution, involves a disappearance of the modulation (13).

Finally, on the crystal edges, one often observes that the characteristic contrast of the 2201-type atomic arrangement disappears at a depth of 10 or 15 Å and is replaced by a contrast typical of a cubic rock-salt-type structure; this feature is always stopped at the level of the double SrO layer of the 0201 unit. An example is shown in Fig. 14. This suggests that bismuth and SrO layers are easily connected, one to the other, or connected to a FeO_2 layer in a mechanism which is similar to that observed in the collapsed bismuth cuprates (25).

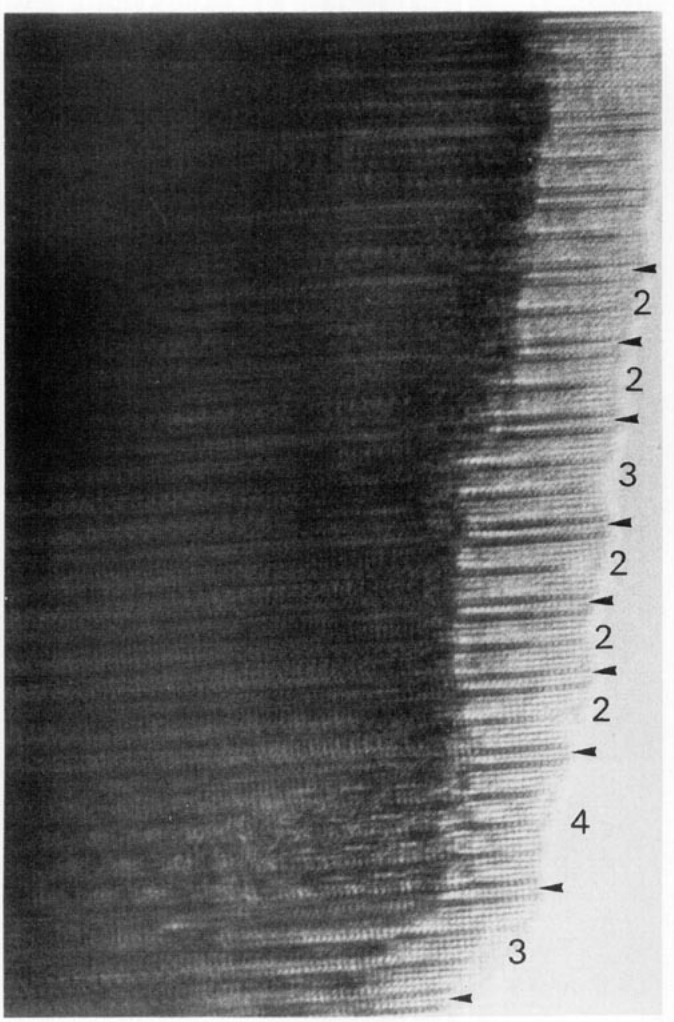

FIG. 13. [110] HREM image showing the existence of aleatory sequences of different members. The numbers indicate the number of adjacent 2201-type slices. The $n = 4$ member exhibits a modulation.

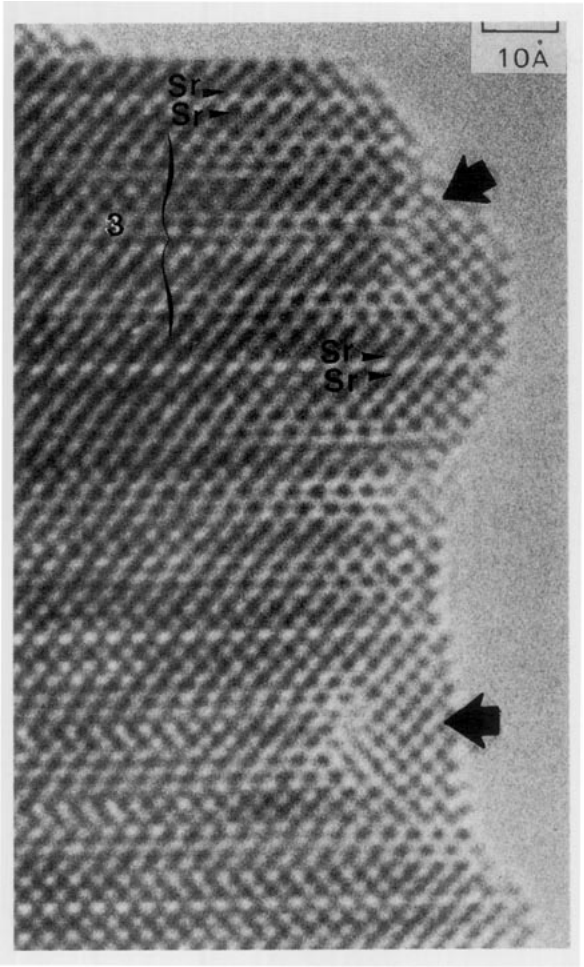

FIG. 14. Enlarged [100] HREM image showing the typical contrast of a cubic rock salt structure (black arrows) observed on the crystal edges.

CONCLUDING REMARKS

This study has allowed a new family of layered ferrites related to the perovskite and rock-salt-type structures, with the ideal formula $Bi_{n+1}Sr_{2n+2}Ba_{n-1}Fe_{n+1}O_{6n+4}$, to be discovered. The parameters and symmetry of the tetragonal subcell of the different members can be predicted according to the following relations:

—$a \approx a_p$ and $c \approx \frac{1}{2}(c_{0201} + nc_{2201})$, with a *P*-type symmetry for odd-*n* members (except $n = 1$ as shown herein), where c_{0201} is the *c* parameter of the 0201 structural unit (close to 12.4 Å) and c_{2201} is that of the 2201 (close to 24.6 Å).

—$a \approx a_p$ and $c \approx c_{0201} + nc_{2201}$ with an *I*-type symmetry for the even-*n* members.

The first important feature that characterizes these 2201–0201 intergrowths deals with the fact that the ideal pure strontium limit phases $Bi_2Sr_2FeO_6$ and Sr_2FeO_4 do not exist in normal conditions of synthesis for reason of charge balance. This favors the formation of intergrowths since it avoids the disproportionation of the system in these two limit members.

The second significant characteristic of these phases deals with the nonstoichiometry that appears on bismuth and barium and seems to favor their stability. The possibility of oxygen nonstoichiometry, either in the form of an excess oxygen in the rock salt layers at the level of bismuth, or in the form of a deficiency leading to the formation of FeO_5 pyramids, should also be considered. The possibility of inducing the mixed valence Fe(III)–Fe(IV) will have to be explored.

The third interesting property concerns the evolution of the modulation of the structure. The first member of the series exhibits an incommensurate modulated structure, as already observed for all pure BiSr cuprates and ferrites (3–11), whereas, in the second and third members, the modulation has disappeared in agreement with the introduction of barium on the bismuth sites, as previously observed for the cuprate $Bi_{1.5}Ba_{2.5}LaCu_2O_8$ (13). The appearance of modulation in the $n \approx 4$ extended defects is in agreement with the decrease of barium content and may be related to an inhomogeneous cationic distribution. Clearly, this study confirms the hypothesis that the presence of barium on the bismuth sites dilates the BiO layers and provides room for the $6s^2$ lone pair of Bi(III), leading to a disappearance of its stereoactivity (13).

In conclusion, the ability of barium to partially occupy the bismuth sites must be considered as the key for the stabilization of such layered compounds. This opens the route to the exploration of new layered oxides built up from transition metal layers and bismuth layers stabilized by the presence of barium. The neutron diffraction study of these oxides, as well as of their magnetic properties, will be carried out.

REFERENCES

1. B. Raveau, C. Michel, M. Hervieu, and D. Groult. "Crystal Chemistry of High Tc Superconducting Copper Oxides," Springer Series in Material Science, 15. Springer-Verlag, Berlin, 1991.
2. J. M. Tarascon, Y. Le Page, W. R. McKinnon, R. Ramesh, M. Eibshutz, E. Tselepis, E. Wang, and G. W. Hull, *Physica C* **167,** 20 (1990).
3. C. Michel, M. Hervieu, M. M. Borel, A. Grandin, F. Deslandes, J. Provost, and B. Raveau, *Z. Phys. B* **68,** 421 (1987).
4. H. Leligny, S. Durcok, P. Labbe, M. Ledesert, and B. Raveau, *Acta Crystallogr. B* 48, 407 (1992).
5. M. Hervieu, C. Michel, N. Nguyen, R. Retoux, and B. Raveau, *Eur. J. Solid State Inorg. Chem.*, **25,** 375 (1988).
6. R. Retoux, C. Michel, M. Hervieu, N. Nguyen, and B. Raveau, *Solid State Commun.* **69,** 599 (1989).
7. H. Maeda, Y. Tanaka, M. Fukutumi, and T. Asano. *Jpn. J. Appl. Phys.* **27,** L209 (1988).
8. C. C. Torardi, M. A. Subramanian, J. C. Calabresse, J. Gopalakrish-

nan, E. M. McCarron, K. J. Morissey, T. R. Askew, R. B. Flippen, U. Choudry, and A. W. Sleight, *Phys. Rev. B* **38,** 225 (1988).
9. M. A. Subramanian, C. C. Torardi, J. C. Calabresse, J. Gopalakrishnan, K. J. Morissey, T. R. Askew, R. B. Flippen, U. Choudry, and A. W. Sleight, *Science* **239,** 1015 (1988).
10. J. M. Tarascon, W. R. McKinnon, P. Barboux, D. M. Hwang, B. G. Bagley, L. H. Greene, G. W. Hull, Y. Le Page, N. Stoffel, and M. Giroud, *Phys. Rev. B* **38,** 8885 (1988).
11. P. Lejay, P. de Rango, A. Sulpice, B. Giordanengo, R. Tournier, R. Retoux, F. Deslandes, C. Michel, M. Hervieu, and B. Raveau, *Rev. Phys. Appl.* **24,** 485 (1989).
12. J. L. Soubeyroux, P. Courbin, L. Fournes, D. Fruchart, and G. Le Flem, *J. Solid State Chem.* **31,** 313 (1980).
13. C. Michel, D. Pelloquin, M. Hervieu, and B. Raveau, *J. Solid State Chem.* **112,** 362 (1994).
14. J. Rodriguez-Carjaval, "Proceedings, Satellite Meeting on Powder Diffraction of the XVth Congress of the International Union of Crystalography, Toulouse, France, July, 1990."
15. G. Mayer-Von Kûrthy, T. Fries, A. Ehmann, and S. Kemmler-Sack. *J. Less-Common Met.* **155,** L19 (1989).
16. P. M. de Wolff, T. Janssen, and A. Janner, *Acta Crystallogr. A* **37,** 625 (1981).
17. H. W. Zandbergen, P. Groen, G. Van Tendeloo, J. Van Landuyt, and S. Amelinckx, *Solid State Commun.* **66,** 397 (1988).
18. V. Caignaert, Ph. Daniel, N. Nguyen, A. Ducouret, D. Groult, and B. Raveau, *J. Solid State Chem.* **112,** 126 (1994).
19. H. Leligny, S. Durcok, Ph. Labbé, M. Ledésert, and B. Raveau, *Acta Cryst. B* **48,** 407 (1992).
20. Y. Matsui, H. Maeda, Y. Tanaka, E. Takayama-Muromachi, S. Takekawa, and S. Horiuchi, *Jpn. J. Appl. Phys.* **27,** L827 (1988).
21. S. Horiuchi, H. Maeda, Y. Tanaka, and Y. Matsui, *Jpn. J. Appl. Phys.* **27,** L1172 (1988).
23. N. Fukushima, S. Nakamura, S. Takeno, M. Hayashi, and K. Endo, *Physica C* **159,** 777 (1989).
24. J. M. Tarascon, Y. Lepage, W. R. Mackinnon, R. Ramesh, M. Eibschutz, E. Tselepis, E. Wang, and G. W. Hull, *Physica C* **167,** 20 (1990).
25. M. Hervieu, M. T. Caldés, D. Pelloquin, C. Michel, S. Cabrera, and B. Raveau, submitted.